inorganics

MDPI

Article

Low-Temperature Ordering in the Cluster Compound $(Bi_8)Tl[AlCl_4]_3$

Maximilian Knies [1], Martin Kaiser [1], Mai Lê Anh [1], Anastasia Efimova [2], Thomas Doert [1] and Michael Ruck [1,3,*]

1 Faculty of Chemistry and Food Chemistry, Technische Universität Dresden, D-01069 Dresden, Germany; Maximilian.knies@tu-dresden.de (M.K.); martin.kaiser@online.de (M.K.); mai.le_anh@tu-dresden.de (M.L.A.); thomas.doert@tu-dresden.de (T.D.)
2 Chair of Inorganic Chemistry, Brandenburg University of Technology Cottbus-Senftenberg, Universitätsplatz 1, D-01968 Senftenberg, Germany; anastasia.efimova@b-tu.de
3 Max Planck Institute for Chemical Physics of Solids, Nöthnitzer Str. 40, D-01187 Dresden, Germany
* Correspondence: michael.ruck@tu-dresden.de

Received: 25 February 2019; Accepted: 18 March 2019; Published: 27 March 2019

Abstract: The reaction of Bi, $BiCl_3$, and TlCl in the ionic liquid $[BMIm]Cl{\cdot}4AlCl_3$ (BMIm = 1-*n*-butyl-3-methylimidazolium) at 180 °C yielded air-sensitive black crystals of $(Bi_8)Tl[AlCl_4]_3$. X-ray diffraction on single crystals at room temperature revealed a structure containing $^1_\infty[Tl(AlCl_4)_3]^{2-}$ strands separated by isolated Bi_8^{2+} square antiprisms. The thallium(I) ion is coordinated by twelve Cl^- ions of six $[AlCl_4]^-$ groups, resulting in a chain of face-sharing $[TlCl_{12}]^{11-}$ icosahedra. The Bi_8^{2+} polycation is disordered, simulating a threefold axis through its center and overall hexagonal symmetry (space group $P6_3/m$). Slowly cooling the crystals to 170 K resulted in increased order in the Bi_8 cluster orientations. An ordered structure model in a supercell with $a' = 2a$, $b' = 2b$, $c' = 3c$ and the space group $P6_5$ was refined. The structure resembles a hexagonal perovskite, with complex groups in place of simple ions.

Keywords: bismuth; cluster compounds; hexagonal perovskite; ionic liquids; low-valent compounds; order–disorder transition; orientational disorder; polycations; pseudosymmetry

1. Introduction

The crystal structure of bismuth monochloride (Bi_6Cl_7), reported by Corbett and Hershaft in 1962 [1], was the first example of a solid containing a homonuclear bismuth polycation. Ever since then, a number of compounds have been synthesized, showing bismuth clusters of various sizes and shapes either isolated [1–7] or coordinating to electron-rich transition metals like Au, Cu, or Ru [8–13]. These cationic clusters typically form in bismuth-rich halide melts. In many cases, an additional Lewis acid—mostly MX_3 with M = Al, Ga and X = Cl, Br, I—was used in the synthesis, resulting in the crystallization of salts, including the corresponding $[MX_4]^-$ anions [14]. The weakly coordinating nature and the high symmetry of these tetrahedral anions enable thermally activated reorientation of the polyhedral bismuth cations. Since the symmetry of the coordination environment of the bismuth polycation is typically higher than its point group, (almost) energetically equivalent orientations can be adopted. Therefore, orientational disorder is a common phenomenon in such structures [2,6,9,10,12,15–17]. This ranges from resolvable disorder on a few alternative positions [12] to the formation of plastic crystals, where the superposition of orientations in time and space creates an averaged electron density resembling a hollow sphere [17].

Herein we report the ionic liquid (IL) [18] based synthesis and structure determination of the bismuth cluster compound $(Bi_8)Tl[AlCl_4]_3$ (**1**). It shows hexagonal pseudosymmetry at room

temperature through a dynamic rotational disorder of Bi_8^{2+} polycations. Upon slowly cooling the crystals to 170 K, the cluster orientations freeze into a long-range ordered superstructure with an enlarged unit cell of lower symmetry.

2. Results and Discussion

2.1. Synthesis and Role of the Ionic Liquid

The reaction of stoichiometric amounts of Bi, $BiCl_3$, and TlCl in the Lewis-acidic ionic liquid [BMIm]Cl·$x$$AlCl_3$ (BMIm = 1-*n*-butyl-3-methylimidazolium; $3 \leq x \leq 5$) at 180 °C resulted in shiny black, air-sensitive, needle-shaped crystals of $(Bi_8)Tl[AlCl_4]_3$ (1). The compound did not form when the same mixture of starting materials was heated in pristine $AlCl_3$. Obviously, the IL is necessary for product formation. Moreover, the amount of $AlCl_3$ used for the formation of the IL plays an important role, as had been observed in previous cases [19]. Empirically, we found that three to five equivalents of $AlCl_3$ per [BMIm]Cl are needed for the successful synthesis of $(Bi_8)Tl[AlCl_4]_3$. The Lewis acidity of the reaction medium as well as the precipitation of solids depend on complex, temperature- and concentration-dependent equilibria including Cl^-, $AlCl_3$, and Lewis acid–base adducts $[Al_nCl_{3n+1}]^-$ (n = 1–3).

2.2. Crystal Structure of $(Bi_8)Tl[AlCl_4]_3$ at Room Temperature

X-ray diffraction on a single crystal revealed that octabismuth(2+)-thallium(I)-tris[tetrachlori doaluminate(III)] crystallizes in the hexagonal space group $P6_3/m$ (no. 176) with two formula units per unit cell and lattice parameters a = 1303.3(1) pm and c = 1039.9(1) pm at room temperature. Atomic parameters and interatomic distances are listed in Tables S1 and S2 of the Supplementary Materials. The crystal structure (Figure 1) is composed of homonuclear, square antiprismatic Bi_8^{2+} polycations, and tetrahedral $[AlCl_4]^-$ ions that are coordinating thallium(I) cations, to form $^1_\infty[Tl(AlCl_4)_3]^{2-}$ strands extending along [001].

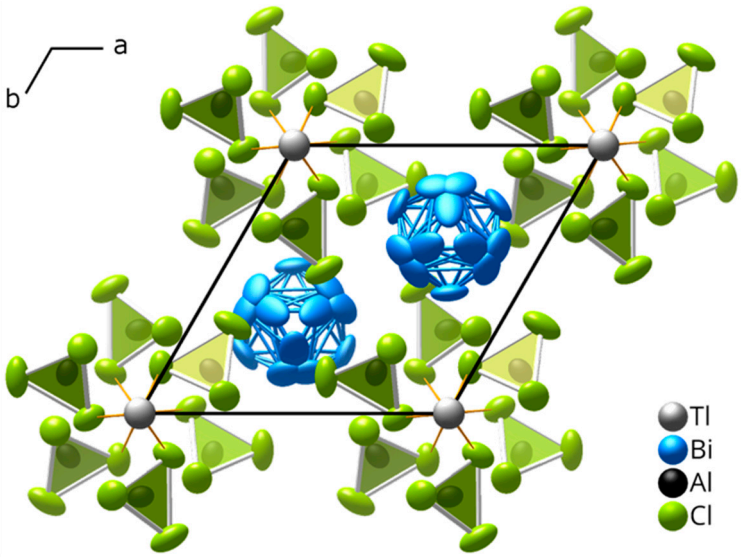

Figure 1. Crystal structure of $(Bi_8)Tl[AlCl_4]_3$ at room temperature along [001]. Bi_8^{2+} square antiprisms show orientational disorder. Ellipsoids comprise 90% of the probability density of the atoms.

The thallium(I) ion on the 6_3 screw axis (point symmetry $\bar{3}$) is surrounded by twelve chloride ions with distances of 337.1(3) pm and 373.8(3) pm, which fall in the range of Tl–Cl distances found in $Tl[AlCl_4]$ (332.0–389.3 ppm) [20]. Six nearer chloride ions form a trigonal antiprism that is expanded to a distorted icosahedron by six more distant chloride ions (Figure 2a). The Tl···Tl distance of 519.9(1) pm suggests no direct interaction between these atoms.

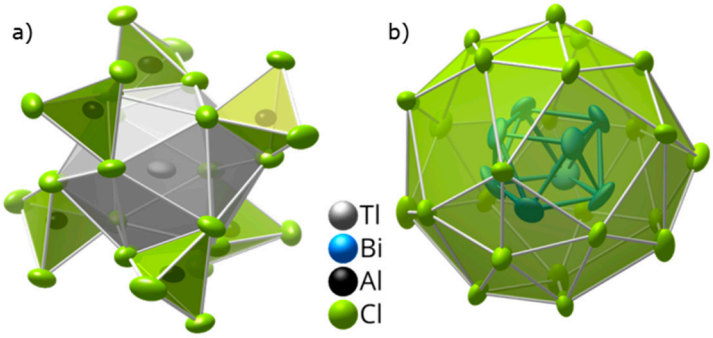

Figure 2. Coordination polyhedra in $(Bi_8)Tl[AlCl_4]_3$: (**a**) distorted $[TlCl_{12}]^{11-}$ icosahedron built from six $[AlCl_4]^-$ tetrahedra; (**b**) distorted snub cube of 24 chloride ions around a Bi_8^{2+} polycation.

The center of gravity of the Bi_8^{2+} polycation is located on the threefold rotation axis (point symmetry $\bar{6}$). This site symmetry does not comply with the D_{4d} symmetry of a square antiprism and thus gives rise to orientational disorder. Extensive structure refinements in space groups with lower symmetry (down to $P112_1$), including (multiple) twinning, did not resolve the apparent disorder (see Supplementary Materials) and no indications for a larger unit cell were found. We thus used space-group symmetry $P6_3/m$ to describe the disordered room temperature structure.

The Bi_8^{2+} polycation, an arachno-cluster according to modified Wade's rules [21], is slightly distorted, showing Bi–Bi distances of 302.5(2) to 307.1(2) pm (average 305.0(2) pm) along the square faces and 305.0(3) to 315.9(2) pm (average 309.6(3) pm) between them. The average distances are slightly shorter than those reported by Beck et al. for $(Bi_8)[AlCl_4]_2$ (309 and 311 pm) [7], which can be attributed to the strong librations that are insufficiently modeled by the harmonic approximations for individually vibrating atoms.

All orientations of the Bi_8^{2+} polycations are equivalent in energy because their anionic surrounding obviously obeys high point group symmetry. A voluminous distorted snub cube—one of the 13 Archimedean solids [22]—consisting of 6 square and 32 triangular faces is formed from 24 chloride ions (Figure 2b). The Bi–Cl distances range from 326(1) to 414(1) pm. This coordination polyhedron is rather uncommon and has, so far, been reported for only a few large organic molecules [23] and intermetallic phases [24–26], and was predicted as the shape of the hypothetical $B_{24}H_{24}^{2-}$ cluster [27].

The average Al–Cl distance of 211.8(6) pm is about 2 pm shorter than the one found in compounds like $Li[AlCl_4]$, $Na[AlCl_4]$, or $K[AlCl_4]$ [28–30]. It shows almost no deviation from the mean distance, which is unusual compared to the abovementioned structures or the Al–Cl distances in $(Bi_8)[AlCl_4]_2$, where at least one distance differs significantly or the $[AlCl_4]^-$ tetrahedra are distorted completely [7].

Furthermore, the room temperature structure of $(Bi_8)Tl[AlCl_4]_3$ can be described by the hexagonal perovskite structure type, first observed in $BaNiO_3$, where each $[AlCl_4]^-$ ion takes the position of the oxide ion, the Ni^{4+} ion is replaced by the Tl^+ ion, and the center of the Bi_8^{2+} polycation is located on the Ba^{2+} position (Figure S1) [31,32]. $(Bi_8)Tl[AlCl_4]_3$ fits that structure type with a Goldschmidt tolerance factor [33] of about 0.86, using a simple geometric approximation for the radial dimensions of $[AlCl_4]^-$ (r_X = 211.8(1) pm) and Bi_8^{2+} (r_A = 254(8) pm), alongside the ionic radius for Tl^+ in twelvefold coordination (r_M = 170 pm) [34]. To the best of our knowledge, $(Bi_8)Tl[AlCl_4]_3$ presents the first example of a perovskite structure containing two complex ions.

2.3. Low-Temperature Structure of $(Bi_8)Tl[AlCl_4]_3$

To decrease the librations and vibrations in the structure, a single crystal was slowly cooled to 170(1) K over a period of 20 h. Additional weak reflections in its diffraction pattern indicated a supercell with $a' = 2a$, $b' = 2b$, and $c' = 3c$ (Figure 3). Furthermore, low-temperature DSC measurements were conducted to determine the ordering temperature. The cooling curve presented no discernable signal, probably due to the nature of the ordering process, where the rotation continuously slows down without any spontaneous lock-in transitions that would be visible in the heat flow.

However, the heating curve revealed a weak endothermic signal at around 200 K which indicated the simultaneous start of rotation of all the clusters (Figure S2).

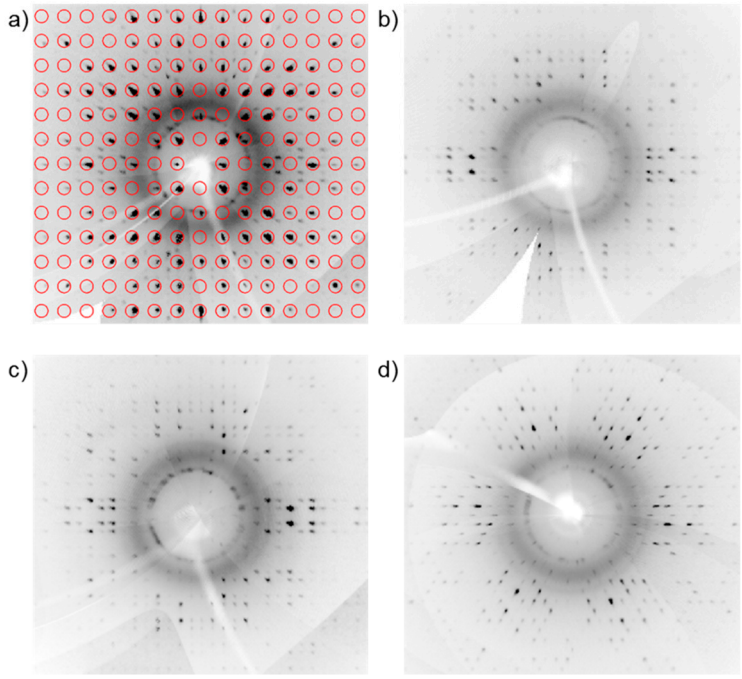

Figure 3. Synthesized precession images of a crystal of $(Bi_8)Tl[AlCl_4]_3$ at 170 K. Additional reflections in the *h*0*l* plane do not correspond to the reflection pattern of the room temperature unit cell (**a**). The 0.5*kl* (**b**), *h*0.5*l* (**c**) and *hk*0.33 (**d**) planes show extensive, symmetric reflection patterns indicating the 2a × 2b × 3c supercell.

The structure refinement revealed a largely, but not fully, ordered structure with the chiral hexagonal space group $P6_5$ (no. 170), which is a subgroup of index 24 of the room temperature space group $P6_3/m$ (Scheme S1). The symmetry reduction is accompanied by the formation of inversion twins (*t*2 transition) as well as antiphase domains (*k*4 and *k*3 transitions). The lattice parameters at 170(1) K are $a = b = 2611.1(2)$ pm and $c = 3122.2(2)$ pm. The unit cell comprises 24 formula units of $(Bi_8)Tl[AlCl_4]_3$. Atomic parameters and interatomic distances are listed in Tables S1 and S2 of the Supplementary Materials.

As can be expected, the basic structure remains the same, but the different orientations of the Bi_8^{2+} polycations are no longer superimposed along the c direction (Figure 4). The 6_5 screw axis runs through the thallium ions with $x \approx y \approx 0$, while there are 2_1 screw axes through the $^1_\infty[Tl(AlCl_4)]^{2-}$ strands with x and/or $y \approx 0.5$. In each column along [001], the three orientations of the Bi_8^{2+} polycations alternate periodically. They still match local mirror symmetry perpendicular to the c-axis, which is, however, not global because of the mismatch with the chiral axis.

Compared to the room temperature structure determination, the distribution of interatomic distances in the bismuth polycations is narrower, with 304.9(1) to 308.9(1) pm (average 306.9(2) pm) along the square faces and 302.2(1) to 310.4(1) pm (average 306.6(3) pm) between them. Although the $^1_\infty[Tl(AlCl_4)]^{2-}$ strands remain virtually unchanged and, above all, preserve the pseudosymmetry of the room temperature structure, the $[AlCl_4]^-$ tetrahedra accommodate the polycation ordering. The Tl–Cl distances now range from 325.8(1) to 366.7(1) pm, showing the expected temperature-induced shortening. The coordination of chloride ions around the bismuth polycations changed considerably. The previously applied description of a snub cube of 24 chloride ions around each cluster would only be applicable if the Bi–Cl distances for attractive interactions were to be extended to a distance of 446.4(1) pm, which corresponds to an increase of over 30 pm compared to the structure at room

temperature. Instead, a smaller number of chloride ions in closer proximity to the polycations dominate, which seems to be key to the long-range order.

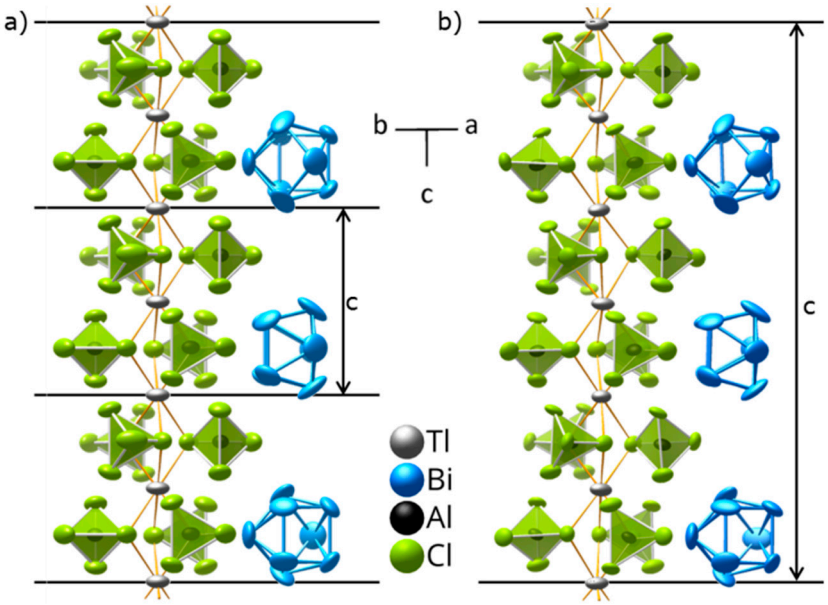

Figure 4. Sections of the crystal structures of $(Bi_8)Tl[AlCl_4]_3$ at room temperature (**a**) and 170 K (**b**) along [110] showing all three possible orientations of the Bi_8^{2+} polycation over the length of $3c_{296K} = c_{170K}$. Ellipsoids comprise 90% of the probability density of the atoms.

3. Materials and Methods

3.1. Synthesis Results and Role of the Ionic Liquid

All compounds were handled in an argon-filled glove box (M. Braun; $p(O_2)/p^0 < 1$ ppm, $p(H_2O)/p^0 < 1$ ppm). The reactions were carried out in silica ampoules with a length of 120 mm and a diameter of 14 mm. The synthesis took place in the ionic liquid $[BMIm]Cl{\cdot}4AlCl_3$, which acted as solvent and reactant. The ampoule was loaded with 23.9 mg TlCl (99%, Sigma Aldrich, St. Louis, MO, USA), 153.1 mg Bi (99.9%, abcr, treated twice with H_2 at 220 °C), 21.3 mg $BiCl_3$ (98%, Alfa Aesar, Karlsruhe, Germany, sublimed three times), 150.4 mg [BMIm]Cl (98%, Sigma-Aldrich, dried under vacuum at 100 °C), and 451.7 mg $AlCl_3$ (sublimed three times). The evacuated and sealed ampoule was heated at 180 °C for 60 h. The ionic liquid turned black at this temperature. Before cooling the mixture to room temperature at $\Delta T/t = -6$ K/h, the ampoule was tilted to enable separation of already precipitated byproducts. Black crystals of $(Bi_8)Tl[AlCl_4]_3$ were obtained alongside colorless $Tl[AlCl_4]$, black $(Bi_8)[AlCl_4]_2$, red $(Bi_5)[AlCl_4]_3$, and colorless $AlCl_3$ in a roughly estimated yield of 40 to 50 wt %. The crystals of **1** could easily be mechanically separated from the byproducts, resulting in a "pure" product with residual IL sticking to the surface, causing a high background in the PXRD analysis (Figure S3). Alternatively, the product was washed three times with dry dichloromethane (DCM), resulting in a mixture whose PXRD diffractogram contained mostly **1** alongside small amounts of $(Bi_8)[AlCl_4]_2$ and a compound we have, so far, been unable to identify (Figure S4) whose reflections were only observed in samples that were treated with DCM. Apparently, the product(s) react with the solvent, forming an impurity in the course of the washing process. Single crystals of **1** were selected for diffraction experiments under inert conditions. The crystals were attached to the tip of glass capillaries (Hilgenberg, Malsfeld, Germany, 0.2 mm inner diameter) with water-free silicon grease (KEL-F®) and encased with another capillary (Hilgenberg, 0.3 mm inner diameter). Both capillaries were molten together on an incandescent Kanthal wire and sealed with picein wax. For powder samples, a capillary (0.3 mm diameter) was filled with powder and sealed using the same procedure.

3.2. EDS Analysis

Energy-dispersive X-ray spectroscopy (EDS) was performed using a SU8020 SEM (Hitachi, Krefeld, Germany) equipped with a silicon drift detector (SDD) X-Max^N (Oxford Cryosystem, Oxford, UK) to check the chemical composition of the crystals. However, several issues impeded the interpretation of the measured data. Since the samples could not be polished, because of their high sensitivity to moisture, the crystal surfaces were not flat, which made finding a suitable surface for the measurement difficult. Furthermore, the $[AlCl_4]^-$ ions partially decompose in the high-energy electron beam (U_a = 30 kV) that is necessary to activate bismuth for this measurement [13]. We thus focused on the ratio between thallium and bismuth. Regarding these values, we were able to support the ratio Tl/Bi = 1:8 within the error of the method. Calculated/experimental Tl/Bi/Al/Cl (atom %) in $(Bi_8)Tl[AlCl_4]_3$ = 4.2:33.3:12.5:50/1.6(3):17(3):30(3):51.6(7).

3.3. X-ray Crystal Structure Determination

Single-crystal X-ray diffraction was performed on a four-circle Kappa APEX II CCD diffractometer (Bruker, Karlsruhe, Germany) with a graphite (002) monochromator and a CCD detector at 296(1) and 170(2) K. Mo Kα radiation (λ = 71.073 pm) was used. Numerical absorption corrections based on an optimized crystal description were applied [35]. The initial structure solution was performed with JANA2006 [36,37]. The structure models were refined with *SHELXL* against F_o^2 [38,39].

3.3.1. Crystallographic Data for $(Bi_8)Tl[AlCl_4]_3$ at 296(1) K

Hexagonal; space group $P6_3/m$ (no. 176); a = 1303.3(1) pm, c = 1039.8(1) pm, V = 1529.7(2) × 10^6 pm^3; Z = 2; $\rho_{calcd.}$ = 5.173 g·cm^{-3}; μ(Mo Kα) = 52.2 mm^{-1}; $2\theta_{max}$ = 50°, $-15 \leq h \leq 16$, $-16 \leq k \leq 15$, $-12 \leq l \leq 12$; 18520 measured, 1077 unique reflections, R_{int} = 0.047, R_σ = 0.023; 63 parameters, R_1[799 $F_o > 4\sigma(F_o)$] = 0.039, wR_2(all F_o^2) = 0.095, GooF = 1.04, min/max residual electron density: −2.10/2.25 e × 10^{-6} pm^{-3}. Every bismuth position is occupied to one-third of its full occupancy, corresponding to the superposition of three orientations of the Bi_8^{2+} polycation. For atomic parameters, see Table S2 of the Supplementary Materials.

3.3.2. Crystallographic Data for $(Bi_8)Tl[AlCl_4]_3$ at 170(2) K

Hexagonal; space group $P6_5$ (no. 170); a = 2611.1(2) pm, c = 3122.2(2) pm; V = 18,433.3(2) × 10^6 pm^3; Z = 24; $\rho_{calcd.}$ = 5.151 g·cm^{-3}; μ(Mo Kα) = 52.0 mm^{-1}; $2\theta_{max}$ = 52.2°, $-31 \leq h \leq 31$, $-31 \leq k \leq 30$, $-37 \leq l \leq 37$; 209738 measured, 21762 unique reflections, R_{int} = 0.169, R_σ = 0.178; 637 parameters, R_1[6278 $F_o > 4\sigma(F_o)$] = 0.049, wR_2(all F_o^2) = 0.058, GooF = 0.932, min/max residual electron density: −2.70/2.07 e × 10^{-6} pm^{-3}. 450 restraints: Three cluster positions show multiple orientations due to an incomplete process of ordering. The first and second positions were described as two clusters with 75.4% and 73.4% probability of occurrence for the main orientation, while the third one is split in three orientations with 54.5%, 23.8%, and 21.7% probability of occurrence, respectively. The Bi–Bi distances were restrained to be equal between equipositional bismuth atoms of each cluster with a 0.2 pm margin of error. Equal atomic displacement parameters were used for corresponding atoms of the $[AlCl_4]^-$ anions, as well as several disordered bismuth atoms. For atomic parameters, see Table S3 of the Supplementary Materials.

Further details of the crystal structure determinations are available from the Fachinformationszentrum Karlsruhe, D-76344 Eggenstein-Leopoldshafen (Germany), E-mail: crysdata@fiz-karlsruhe.de, upon quoting the depository numbers CSD-1898840 (296 K) and 1898841 (170 K).

3.4. Differential Scanning Calorimetry

In an argon-filled glove box (MBraun UNIlab, Garching, Germany), 20.73 mg of the sample was loaded and sealed in an Al container (40 μL). Heat-flux differential scanning calorimetry (DSC) was performed using a DSC 204 F1 Phoenix (Netzsch, Selb, Germany) in the temperature range from 109

to 283 K, with heating and cooling rates of 2 K/min under a dry N_2 atmosphere. The characteristic temperature derived from the DSC curve was an extrapolated onset temperature.

4. Conclusions

The new bismuth-rich metalate $(Bi_8)Tl[AlCl_4]_3$ consists of $^1_\infty[Tl(AlCl_4)]^{2-}$ strands and isolated Bi_8^{2+} polycations. The latter shows dynamic disorder at room temperature but order upon slow cooling to 170 K. Similar dynamics had been observed in other compounds with isolated polyhedral ions [2,6,9,10,12,15–17]. However, in most of those cases, cooling led either to a freezing of dynamic to static disorder or to low symmetric structures with enormously enlarged unit cells and multiple twinning that could not be resolved. The comparatively smooth ordering of $(Bi_8)Tl[AlCl_4]_3$ can thus be regarded a stroke of luck.

Supplementary Materials: The following are available online at http://www.mdpi.com/2304-6740/7/4/45/s1, Figure S1: Representation of structural motifs in $BaNiO_3$ and $Bi_8Tl[AlCl_4]_3$ according to the hexagonal perovskite structure type. Figure S2: Low-temperature DSC measurement of a sample of $(Bi_8)Tl[AlCl_4]_3$. Figure S3: Powder diffractogram of a sample of $Bi_8Tl[AlCl_4]_3$ crystals without further treatment. Figure S4: Powder diffractogram of the product of a $Bi_8Tl[AlCl_4]_3$ synthesis after treatment with dry DCM. Scheme S1: Simplified Bärnighausen tree for the symmetry descent at low temperatures. **Table S1**: Selected interatomic distances in $(Bi_8)Tl[AlCl_4]_3$, Table S2: Coordinates and coefficients of the tensors of the anisotropic displacement and equivalent displacement parameters for the atoms in $(Bi_8)Tl[AlCl_4]_3$. Table S3: Coordinates and coefficients of the tensors of the anisotropic displacement, and equivalent displacement parameters for the atoms in $(Bi_8)Tl[AlCl_4]_3$ at 170(2) K. CIF and the checkCIF output files.

Author Contributions: Conceptualization, M.K. (Maximilian Knies) and M.R.; validation, M.K. (Maximilian Knies); investigation, M.K. (Maximilian Knies), M.K. (Martin Kaiser) and M.L.A.; resources, M.R.; data curation, M.K. (Maximilian Knies), M.L.A. and A.E.; writing—original draft preparation, M.K. (Maximilian Knies); writing—review and editing, M.R.; visualization, M.K. (Maximilian Knies) and M.K. (Martin Kaiser); supervision, T.D. and M.R.; project administration, M.R.; funding acquisition, M.R.

Funding: This research was funded by the Deutsche Forschungsgemeinschaft (DFG), grant number SPP 1708.

Acknowledgments: We acknowledge administrative support by Alina Markova and technical support by Michaela Münch and Andrea Brünner.

Conflicts of Interest: The authors declare no conflict of interest.

References

1. Hershaft, A.; Corbett, J.D. Crystal Structure of Bismuth Monochloride. *J. Chem. Phys.* **1962**, *36*, 551–552. [CrossRef]
2. Ruck, M.; Steden, F. Bi_5^{3+}-Polykationen in geordneten und plastischen Kristallen von $Bi_5[AlI_4]_3$ und $Bi_5[AlBr_4]_3$. *Z. Anorg. Allg. Chem.* **2007**, *633*, 1556–1562. [CrossRef]
3. Fischer, A.; Lindsjö, M.; Kloo, L. Improvements of and Insights into the Isolation of Bismuth Polycations from Benzene Solution—Single-Crystal Structure Determinations of $Bi_8[GaCl_4]_2$ and $Bi_5[GaCl_4]_3$. *Eur. J. Inorg. Chem.* **2005**, *2005*, 670–675. [CrossRef]
4. Corbett, J.D. Homopolyatomic ions of the heavy post-transition elements. Preparation, properties, and bonding of $Bi_5(AlCl_4)_3$ and $Bi_4(AlCl_4)$. *Inorg. Chem.* **1968**, *7*, 198–208. [CrossRef]
5. Ahmed, E.; Köhler, D.; Ruck, M. Room-Temperature Synthesis of Bismuth Clusters in Ionic Liquids and Crystal Growth of $Bi_5(AlCl_4)_3$. *Z. Anorg. Allg. Chem.* **2009**, *635*, 297–300. [CrossRef]
6. Hampel, S.; Schmidt, P.; Ruck, M. Synthese, thermochemische Eigenschaften und Kristallstruktur von Bi_7Cl_{10}. *Z. Anorg. Allg. Chem.* **2005**, *631*, 272–283. [CrossRef]
7. Beck, J.; Brendel, C.J.; Bengtsson-Kloo, L.; Krebs, B.; Mummert, M.; Stankowski, A.; Ulvenlund, S. The Crystal Structure of $Bi_8(AlCl_4)_2$ and the Crystal Structure, Conductivity, and Theoretical Band Structure of Bi_6Cl_7 and Related Subvalent Bismuth Halides. *Chem. Ber.* **1996**, *129*, 1219–1226. [CrossRef]
8. Ruck, M. $Bi_{24}Ru_3Br_{20}$: Ein pseudo-tetragonales Subbromid mit $[RuBi_6Br_{12}]$-Clustern und $[Ru_2Bi_{17}Br_4]$-Gruppen. *Z. Anorg. Allg. Chem.* **1997**, *623*, 1591–1598. [CrossRef]

9. Wahl, B.; Ruck, M. Die molekularen Cluster $[Bi_{10}Au_2](EBi_3X_9)_2$ (E = As, Bi; X = Cl, Br)—Synthese, Kristallstrukturen, Drillingsbildung und chemische Bindung. *Z. Anorg. Allg. Chem.* **2008**, *634*, 2267–2275. [CrossRef]
10. Groh, M.F.; Isaeva, A.; Frey, C.; Ruck, M. $[Ru(Bi_8)_2]^{6+}$—A Cluster in a Highly Disordered Crystal Structure is the Key to the Understanding of the Coordination Chemistry of Bismuth Polycations. *Z. Anorg. Allg. Chem.* **2013**, *639*, 2401–2405. [CrossRef]
11. Groh, M.F.; Isaeva, A.; Ruck, M. $[Ru_2Bi_{14}Br_4](AlCl_4)_4$ by Mobilization and Reorganization of Complex Clusters in Ionic Liquids. *Chem. Eur. J.* **2012**, *18*, 10886–10891. [CrossRef] [PubMed]
12. Knies, M.; Kaiser, M.; Isaeva, A.; Müller, U.; Doert, T.; Ruck, M. The Intermetalloid Cluster Cation $(CuBi_8)^{3+}$. *Chem. Eur. J.* **2018**, *24*, 127–132. [CrossRef] [PubMed]
13. Müller, U.; Isaeva, A.; Richter, J.; Knies, M.; Ruck, M. Polyhedral Bismuth Polycations Coordinating Gold(I) with Varied Hapticity in a Homoleptic Heavy-Metal Cluster. *Eur. J. Inorg. Chem.* **2016**, *2016*, 3580–3584. [CrossRef]
14. Ruck, M.; Locherer, F. Coordination chemistry of homoatomic ligands of bismuth, selenium and tellurium. *Coord. Chem. Rev.* **2015**, *285*, 1–10. [CrossRef]
15. Groh, M.F.; Müller, U.; Isaeva, A.; Ruck, M. Ionothermal Syntheses, Crystal Structures, and Chemical Bonding of the Rhodium-Centered Clusters $[RhBi_9]^{4+}$ and $[(RhBi_7)I_8]$. *Z. Anorg. Allg. Chem.* **2017**, *643*, 1482–1490. [CrossRef]
16. Groh, M.F.; Wolff, A.; Wahl, B.; Rasche, B.; Gebauer, P.; Ruck, M. Pentagonal Bismuth Antiprisms with Endohedral Palladium or Platinum Atoms by Low-Temperature Syntheses. *Z. Anorg. Allg. Chem.* **2017**, *643*, 69–80. [CrossRef]
17. Wosylus, A.; Dubenskyy, V.; Schwarz, U.; Ruck, M. Dynamic Disorder of Bi_8^{2+} Clusters in the Plastic Phase $(Bi_8)_3Bi[InI_4]_9$. *Z. Anorg. Allg. Chem.* **2009**, *635*, 1030–1035. [CrossRef]
18. Wilkes, J.S. *Ionic Liquids in Synthesis*, 2nd ed.; Wasserscheid, P., Welton, T., Eds.; Wiley-VCH: Weinheim, Germany, 2007; pp. 1–6.
19. Estager, J.; Holbrey, J.D.; Swadźba-Kwaśny, M. Halometallate ionic liquids—Revisited. *Chem. Soc. Rev.* **2014**, *43*, 847–886. [CrossRef] [PubMed]
20. Timofte, T.; Mudring, A.-V. A Systematic Study on the Crystal Structures of $TlMX_4$ (M = Al, Ga; X = Cl, Br, I). *Z. Anorg. Allg. Chem.* **2009**, *635*, 840–847. [CrossRef]
21. Wade, K. Structural and Bonding Patterns in Cluster Chemistry. *Adv. Inorg. Chem. Radiochem.* **1976**, *18*, 1–66. [CrossRef]
22. Wenninger, M.J. *Polyhedron Models*; Cambridge University Press: Cambridge, UK, 1971; pp. 20–32. [CrossRef]
23. MacGillivray, L.R.; Atwood, J.L. A chiral spherical molecular assembly held together by 60 hydrogen bonds. *Nature* **1997**, *389*, 469–472. [CrossRef]
24. Shoemaker, D.P.; Marsh, R.E.; Ewing, F.J.; Pauling, L. Interatomic distances and atomic valences in $NaZn_{13}$. *Acta Crystallogr.* **1952**, *5*, 637–644. [CrossRef]
25. Xie, W.; Cava, R.J.; Miller, G.J. Packing of Russian doll clusters to form a nanometer-scale CsCl-type compound in a Cr–Zn–Sn complex metallic alloy. *J. Mater. Chem. C* **2017**, *5*, 7215–7221. [CrossRef]
26. McElfresh, M.W.; Hall, J.H.; Ryan, R.R.; Smith, J.L.; Fisk, Z. Structure of the heavy-fermion superconductor UBe_{13}. *Acta Crystallogr. Sect. C* **1990**, *46*, 1579–1580. [CrossRef]
27. Oliva, J.M.; Vegas, Á. Merging boron solid state and molecular chemistry: Energy landscapes in the exo/endo closo-borane complex $Sc[B_{24}H_{24}]^+$. *Chem. Phys. Lett.* **2012**, *533*, 50–55. [CrossRef]
28. Perenthaler, E.; Schulz, H.; Rabenau, A. Die Strukturen von $LiAlCl_4$ und $NaAlCl_4$ als Funktion der Temperatur. *Z. Anorg. Allg. Chem.* **1982**, *491*, 259–265. [CrossRef]
29. Baenziger, N.C. The crystal structure of $NaAlCl_4$. *Acta Crystallogr.* **1951**, *4*, 216–219. [CrossRef]
30. Mairesse, G.; Barbier, P.; Wignacourt, J.-P. Potassium tetrachloroaluminate. *Acta Crystallogr. Sect. B* **1978**, *34*, 1328–1330. [CrossRef]
31. Takeda, Y.; Kanamura, F.; Shimada, M.; Koizumi, M. The crystal structure of $BaNiO_3$. *Acta Crystallogr. Sect. B* **1976**, *32*, 2464–2466. [CrossRef]
32. Lander, J.J. The crystal structures of NiO·3BaO, NiO·BaO, $BaNiO_3$ and intermediate phases with composition near $Ba_2Ni_2O_5$; with a note on NiO. *Acta Crystallogr.* **1951**, *4*, 148–156. [CrossRef]
33. Goldschmidt, V.M. Die Gesetze der Krystallochemie. *Naturwissenschaften* **1926**, *14*, 477–485. [CrossRef]

34. Shannon, R.D. Revised effective ionic radii and systematic studies of interatomic distances in halides and chalcogenides. *Acta Crystallogr. Sect. A* **1976**, *32*, 751–767. [CrossRef]
35. Hahn, F. *X-Shape, Crystal Optimization for Numerical Absorption Correction Program*; Stoe & Cie GmbH: Darmstadt, Germany, 2008.
36. Petricek, V.; Dusek, M.; Palatinus, L. *JANA2006, The Crystallographic Computing System*; Institute of Physics: Praha, Czech Republic, 2011.
37. Palatinus, L.; Chapuis, G. *SUPERFLIP*—A computer program for the solution of crystal structures by charge flipping in arbitrary dimensions. *J. Appl. Cryst.* **2007**, *40*, 786–790. [CrossRef]
38. Sheldrick, G.M. *SHELXL, Program for Crystal Structure Refinement—Multi-CPU*; Georg-August-Universität Göttingen: Göttingen, Germany, 2014.
39. Sheldrick, G.M. A short history of *SHELX*. *Acta Crystallogr. Sect. A* **2008**, *64*, 112–122. [CrossRef] [PubMed]